Visualization of the Fibrous Structure of the Heart

T.H.J.M. Peeters*, A. Vilanova*, G.J. Strijkers†, and B.M. ter Haar Romeny*

*Biomedical Image Analysis †Biomedical NMR
Department of Biomedical Engineering
Technische Universiteit Eindhoven
Den Dolech 2, Eindhoven, Netherlands
Email: {T.Peeters, A.Vilanova, G.J.Strijkers, B.M.terHaarRomeny}@tue.nl

Abstract

There is need for detailed knowledge about the changes in the structure of the muscle fibers of the heart after an ischemic infarction. In order to improve the treatment of this illness, it is crucial to understand the adaptation of the structure. Diffusion Tensor Imaging (DTI) is a non-destructive technique that can be used to reconstruct the structure of the fibers in the heart wall.

The visualization of this vast amount of densely packed fibers is a challenging problem. In order to understand the structure, it is necessary to convey both the shapes of the fibers, and their mutual coherency. We propose to use line illumination and shadowing of fibers in order to improve the perception of their structure. Using these methods, we present an intuitive way to visualize the structure together with other properties, while avoiding cluttering.

The presented methods were applied to a series of healthy and ischemic mouse hearts. These methods helped the user to gain insight in the fibrous structure of the heart.

1 Introduction

The heart is a hollow muscle that pumps blood through the body by repeated, rhythmic contractions. In mammals, it has four chambers: the two upper atria and the two lower ventricles. As opposed to skeletal muscle, the heart contracts without being triggered by nerve impulses, and it can work continuously without fatigue. The efficiency of the heart as a pump is the result of the arrangement of the muscle fibers in the heart wall. This cardiac structure is not fully understood and has been a topic of research and discussion for at least a few hundred years. Even today it is a disputed topic [2].

The oxygen needed by the heart muscle to do its work is supplied through blood coming from the coronary arteries. A restriction of this blood supply is called *cardiac ischemia*. Acute cardiac ischemia, commonly known as a heart attack, can be caused by a blood clot occluding a coronary artery. If a heart attack is survived, a wound healing process takes place. This usually causes a local thinning of the heart wall and changes in its fibrous structure. In non-ischemic regions, the heart wall may thicken to compensate for the loss of functional muscle fibers in the ischemic region. If these changes cannot compensate for physiological needs of the body, heart failure can occur. Because the changes are not fully understood, research is being done with the purpose of improving our insight in the fibrous structure of both healthy and ischemic hearts. The long-term goal of this research is to improve treatment of cardiac infarction.

One of the tools that are used to characterize the heart is Diffusion Tensor Imaging (DTI) to image healthy and ischemic mouse hearts. DTI is an MRI technique that measures the local diffusion of water in tissue. The measured diffusion provides information on the presence and orientation of fibrous structures in tissue (e.g. in heart muscle). DTI is an improvement over conventional histological techniques, because it is not destructive and less labor-intensitive [6]. However, like histology, heart DTI cannot be applied in-vivo in mice. The reason for this is that the movement of the heart interferes with the diffusion of water that is being measured.

A common way to visualize DTI data is by reconstructing fibers using tractography [14]. Most existing tools for visualizing DTI fibers render them either as unshaded polylines or as polygonal tubes.

The use of unshaded lines gives no cues about the shape of the fibers, as is shown in figures 3(a) and 4(a). The use of polygonal tubes requires a large number of polygons in order to achieve high image quality (figure 4(b)). This results in bad rendering performance. Also, neither method conveys the coherent structure of a large amount of fibers clearly. For heart visualization this is very important because the heart wall is densely packed with a vast amount of fibers with a continuously changing orientation when moving through the tissue.

We apply techniques that are used for the realistic rendering of human hair in order to improve the visualization of the dense fibrous structures of the heart. The two most important components of realistic hair rendering are the local lighting model, and the casting of shadows from hair fibers onto each other. Both techniques are essential for creating realistically-looking images [7]. Without proper line lighting, individual fiber shapes are not apparent. Without shadowing, the coherent structure of groups of fibers cannot be easily shown.

In scientific visualization, illuminated lines are also used to acquire a better perception of shape [12, 10]. The lighting model used is similar to that used for hair rendering. However, it is not combined with shadowing. In this paper, we show how perception of both shape and coherency of large amounts of densely packed fibers can be considerably improved by applying line lighting and shadowing. We then apply them to fibers tracked in DTI datasets of healthy and diseased hearts. We also introduce a new approach to visualizing a slice of DTI heart data. We render short fibers originating from the selected slice in order to show the fibrous structure in the slice. This can be considered as a hybrid method where fiber tracking is used to create a glyph-like representation of the local structure. Our technique improves existing tools to analyze heart data in the sense that the fibrous structure is visualized in a more intuitive way, and it can be combined with the visualization of additional properties using color coding. Because we implemented the lighting and shadowing to run directly on the GPU, we achieve interactive framerates.

General methods for visualizing DTI data, and specific methods used for heart visualization are given in section 2. In section 3, we describe our methods for the visualization of DTI heart data. In section 4 we apply our method to a series of healthy and ischemic mouse hearts and we analyze the results. Finally, in section 5, we summarize our contributions and identify directions for future research.

2 Background and related work

A DTI dataset consists of a structured grid, with a *diffusion tensor* on each grid point representing the local diffusion. Each diffusion tensor is represented by a symmetric 3×3 positive definite matrix $\mathbf{D}$. Trilinear interpolation on each component of $\mathbf{D}$ is used to reconstruct a continuous tensor field. Other interpolation methods might be used for interpolating tensors, but that topic is beyond the scope of this paper.

Eigenanalysis of $\mathbf{D}$ gives the eigenvalues $\lambda_1 \geq \lambda_2 \geq \lambda_3 \geq 0$, and the accompanying eigenvectors $\vec{e}_1, \vec{e}_2$ and $\vec{e}_3$. The eigenvectors represent the principal diffusion directions, and the eigenvalues are the corresponding diffusion coefficients. An intuitive way of representing a diffusion tensor is with an ellipsoid that has its axes aligned with the eigenvectors of $\mathbf{D}$ and scaled by the eigenvalues.

Many measures or *anisotropy indices* exist for classifying the diffusion type [14]. In this paper we use fractional anisotropy (*FA*) defined by:

$$FA = \frac{\sqrt{(\lambda_1 - \lambda_2)^2 + (\lambda_2 - \lambda_3)^2 + (\lambda_1 - \lambda_3)^2}}{\sqrt{2(\lambda_1^2 + \lambda_2^2 + \lambda_3^2)}}$$

Various methods exist for visualizing DTI data [14]. One can compute scalar anisotropy indices such as *FA* from the diffusion tensors. The resulting scalar volume can be visualized by, for example, volume rendering. Less information is lost if the tensor field is simplified to the vector field defined by $\vec{e}_1$. A popular way to visualize this field is by slicing the data and applying RGB color coding. This color coding directly maps the components of $\vec{e}_1$ to RGB color space.

An often-used measure that enables quantification of fiber orientations in the heart is the *helix angle* α_h. It represents the angle between the fiber direction and the plane perpendicular to the long-axis of the heart. This is shown in figure 1. α_h is often used as input of models for heart simulation, and for quantification of deviations in fiber orientations between healthy and diseased hearts. Figure 5(a) shows α_h in one slice of a healthy heart using color coding.

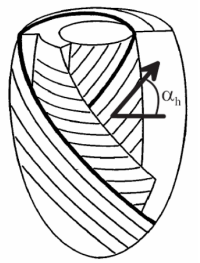

Figure 1: Schematic representation of the fiber orientations in the left ventricle of the heart with a depiction of the helix angle α_h.

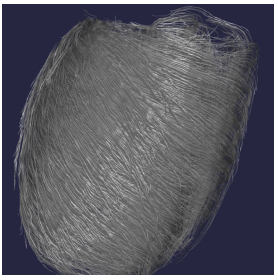

Figure 2: Long fibers tracked in a healthy mouse heart using whole-volume seeding. Line lighting and shadowing were used to render the fibers.

Tractography or *fiber tracking* aims at reconstructing the fibrous structure that lies at the basis of the anisotropy measured by DTI. There are several techniques to perform this reconstruction. We use streamline tracing in the vector field of $\vec{e}_1$. It is the same method as described by Vilanova et al. [13]. Streamline tracing is initialized from *seed points* that specify the starting positions of the fibers. Several strategies exist for the placement of seed points. These *seeding strategies* require a varying degree of input from the user. If the user has to specify a region of interest (ROI) where seedpoints are placed, it is possible that important features of a dataset are missed. If automatic seeding in the whole volume is used, the resulting fibers can clutter the image (see figure 2). This makes it difficult to get insight in the data. User-defined ROIs can also be used to select a subset of fibers from a large set of precomputed fibers. It has been shown that this can be helpful for the exploration and interpretation of DTI brain data [1, 4].

The fibers that are the output of a fiber tracking algorithm can be visualized in various ways. The simplest way to visualize them is with unshaded lines, as is shown in figures 3(a) and 4(a). Local anisotropy indices can be color-coded on the lines. However, with unshaded lines it is hard to see their actual shapes and their mutual coherencies. In order to improve the perception of shape and orientation of the fibers, the local fiber orientation can be color-coded on the lines by mapping the components of the local direction directly to RGB values. Zhukov and Barr [18] propose a color coding that distinguishes between muscle fibers in the heart that follow either a clockwise or a counter-clockwise spiral trajectory. However, using color coding to improve the perception of the fiber structure prohibits the use of color to show other properties.

Polygonal tubes can be used to represent fibers, but in order to achieve a good image quality, a large number of polygons is required. This results in bad rendering performance. For dense sets of fibers, polygonal tubes also cause more occlusion than line-based techniques. Polygonal tubes are shown in figure 4(b).

In order to visualize DTI heart data, color maps of 2D heart slices based on various scalar indices (e.g. α_h and *FA*) are applied [6]. This is shown in figures 5(a) and 5(d). Fiber tracking and glyphing have also been used to visualize DTI heart data [18, 11]. However, these visualizations tend to use only whole-volume seeding for fiber tracking in order to reconstruct the heart shape. Using this technique it is hard to say anything about the structure of fibers inside the heart wall because they are occluded. The glyphing approaches can only show local information in a limited region of interest. If glyphs are distributed densely, occlusion becomes a serious problem. Already when showing the glyphs in a 2D slice, they become ineffective and color coding is necessary to indicate orientation.

In hair rendering, anisotropic lighting [7, 3] is used for the local shading model. This gives realistic-looking results and conveys the fiber shapes to the viewer in an intuitive way. Some scientific visualizations use illuminated lines in order to make the shapes of the individual lines easier to interpret [10]. Stalling et al. [12] describe a method that uses the normal in the normal plane of the fiber that maximizes the lighting intensity as an efficient model for anisotropic lighting. Wenger et

al. [15] use anisotropic lighting for volume rendering of vector-field structure and also apply it to DTI. However, the density of the fibers that can be visualized is limted by the resolution of the 3D texture that they use for hardware-accelerated volume rendering.

The large number of algorithms for rendering of shadows [17] indicates the importance of shadows for creating realistic-looking scenes. For rendering hair and fur, self-shadowing is essential to make it look real [7]. Shadow mapping is an image-space shadowing technique that is suitable for complex scenes because it does not depend on the geometric complexity of the scene [16]. However it has some problems, including aliasing on the edges of casted shadows. Therefore, many extensions to the classical shadow mapping algorithm exist, of which some were especially constructed for the rendering of complex structures such as hair [9, 8].

We apply techniques used for the realistic rendering of hair in order to create a better visualization of DTI heart data. We apply anisotropic lighting in order to make the shapes of the fibers better visible. Shadow mapping is applied to make the coherent structure of nearby fibers apparent. In addition, we track short fibers from seed points in one slice. This avoids the occlusion and cluttering caused by tracking long fibers with whole-volume seeding. Compared with glyph-based methods, it shows more context and suffers less from occlusion because the fibers are only one pixel thick. We also combine our method with color coding to visualize addtional properties such as *FA*. Because interaction is essential for the inspection of the heart data, we make use of the capabilities of the GPU to implement our techniques such that interactive framerates are possible.

3 Heart-structure visualization

In this section, we show how proper lighting and shadowing can be used to improve the visual perception of the structure of a DTI dataset. We then present a method to visualize slices of DTI heart data that can show the fiber structure and additional properties, while avoiding cluttering. In section 3.1, we describe how existing line lighting theory is implemented for use with DTI fibers. In section 3.2, we explain how the standard shadow mapping technique is modified in order to give good results for dense line datasets. Finally, in section 3.3 we describe the slice visualization. The lighting and shadowing algorithms are implemented in the OpenGL Shading Language (GLSL), and run directly on the GPU. This ensures interactive rendering speeds.

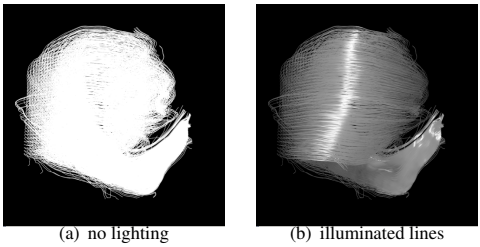

(a) no lighting (b) illuminated lines

Figure 3: Fibers tracked in a folded eye nerve of a pig, which was used to create a phantom DTI dataset.

3.1 Illuminated lines

In the Phong lighting model, the light intensity I at a point on a surface, follows the equation:

$$I = k_a + k_d(\vec{L}\cdot\vec{N}) + k_s(\vec{V}\cdot\vec{R})^n \quad (1)$$

The material-specific values of k_a, k_d, k_s and n are the ambient, diffuse and specular coefficients, and the specular component or shininess. $\vec{N}$ is the normal at the surface point. $\vec{L}$ points towards the light source, $\vec{V}$ towards the camera position, and $\vec{R}$ is the reflection of $\vec{L}$ at $\vec{N}$. Vectors $\vec{N}$, $\vec{L}$, $\vec{V}$, and $\vec{R}$ have unit length.

This model cannot be applied to illuminate lines directly, because lines do not have a single normal $\vec{N}$, but a plane of normals perpendicular to the tangent direction $\vec{T}$. This problem can be resolved by choosing for $\vec{N}$ the vector in the normal plane that maximizes $(\vec{L}\cdot\vec{N})$ and $(\vec{V}\cdot\vec{R})$ in Eq. (1). To avoid explicit calculation of the optimal $\vec{N}$, the following equations can be used [3, 12]:

$$\vec{L}\cdot\vec{N} = \sqrt{1-(\vec{L}\cdot\vec{T})^2} \quad (2)$$

$$\vec{V}\cdot\vec{R} = (\vec{L}\cdot\vec{N})\sqrt{1-(\vec{V}\cdot\vec{T})^2} - (\vec{L}\cdot\vec{T})(\vec{V}\cdot\vec{T}) \quad (3)$$

Using Eq. (2) and (3), the calculation of I in Eq. (1) can be implemented directly as a GLSL shader. The effect of line lighting is shown in figure 3.

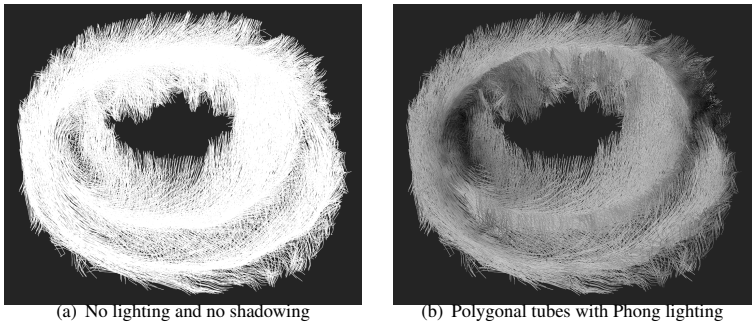

(a) No lighting and no shadowing (b) Polygonal tubes with Phong lighting

(c) Line lighting and no shadowing (d) Line lighting and shadowing

Figure 4: Short fibers tracked in a slice of a healthy heart dataset. In (b) fibers are represented by polygonal tubes with 6 sides.

3.2 Shadowing

Shadow mapping [16] is a well-known and well-researched technique. It has two render passes. In the first render pass it renders the scene with the camera placed at the light source. The depth-values in *light-coordinates* of the rendered fragments are stored in the *shadow map*. In the second render pass, the camera is placed at the actual view position. For each fragment, the view-coordinates are converted to light-coordinates (x,y,z). The z-component is then compared to the depth-value z_s stored in the shadow map at position (x,y). If $z = z_s$ then the current fragment is visible from the light source and thus lighted. If $z > z_s$ then there is another object closer to the light source that obscures the current fragment, so it must be shadowed.

This approach has two problems. The first is the limited resolution of the shadow map combined with the computations to convert coordinates in camera space to light space. One pixel in the shadow map may represent many pixels in the image in camera space. This can cause serious aliasing artefacts. The second problem is self-shadowing of objects. Because they are the result of two different, limited-precision computations, the depth-values z and z_s will not be exactly the same. Depending on which value is larger, for each fragment there is a chance that the object casts a shadow onto itself. This problem is usually solved by subtracting an offset d from z_s, such that the computed distance between z and z_s must be at least d for the fragment to be shadowed. This is not a solution in our case because we have very dense sets of fibers where no reasonable value can be given for d.

We tackle the aliasing problem by using a high-resolution shadow map. We implemented the shadow-mapping technique using Framebuffer Objects to render the shadow map to a texture which is at least twice as large as the resulting on-screen image, in each dimension. Our current graphics card supports textures of up to 4096^2 pixels. The use of these high-resolution textures for shadow maps, suffiently reduces the aliasing problem in our application.

The problem with lines casting shadows onto

themselves is solved by not using depth-values for the shadow computations, but a unique identifier id_l for each line segment. These id_l-values are rendered to the shadow map and compared with the fiber id_ls when rendering the scene with the camera placed at the actual view position.

In figure 4, the image with shadows makes the coherent structure of the fibers visible. Without shadowing, in figure 4(c), it is nearly impossible to determine which fibers are in front and which are behind. By applying shadowing in figure 4(d), fibers that are behind other fibers are deemphasized. This makes it easier for the viewer to determine which fibers are in front, and which are behind. Notice that lighting and shadowing are more effective communicating the fiber structure when interactive changes of view are used.

3.3 Slice visualization

Current practice for visualizing heart slices is to use glyphing, or color coding of anisotropy indices (figure 5(d)) or fiber orientation (figure 5(a)). These approaches have some disadvantages. Color coding can visualize at most a few scalar components in a 2D subset of the data. Glyphing can only show local information in a limited region of interest.

Our approach of rendering fibers with lighting and shadowing, makes it possible to visualize the shape and orientation of fibers, and to show the coherency among densely structured fibers. The use of anisotropic lighting and shadowing was inspired by the realistic rendering of human hair. If the rendered hair are short, viewers will intuitively interpret the structure of the hair, including the local fiber orientations. We apply this to slices in heart DTI data by using fiber tracking to reconstruct short fibers that pass through the current slice of interest. This is done by placing a dense set of evenly-spaced seeding points in the specified slice. Fibers are then tracked with a small maximum length. Results for a healthy heart are shown in figures 5 and 4.

This approach has several advantages. First, our method is more intuitive than color coding to show the local fiber orientation. Color coding of the fiber orientation will need a legenda that relates the colors to orientations in order to interpret the images. Second, color coding (e.g. color coding of α_h in figure 5(a)) cannot show all components of $\vec{e}_1$ while retaining a unique color for each orientation. Third, our method can be combined with color coding to show additional information. Since colors are not used for showing the fiber orientation, anisotropy indices can be encoded using color. This is shown for *FA* in figure 5(c). Finally, the length of the fibers can be varied. This can be used to give the user control over the amount of information that is being shown.

4 Results

We applied the proposed visualization to a series of healthy and infarcted mouse hearts. Four datasets were available of healthy hearts. For infarcted hearts we had 5, 4 and 5 datasets measured respectively at 7, 14 and 28 days after infarction. Each heart is only a few millimeters long and the scanning resolution was $117 \times 117 \times 234 \mu m^3$. Because DTI acquisition of a mouse heart cannot be done *in-vivo*, no two different datasets represent the same actual heart. The infarcted hearts had an ischemic infarction in the left ventricle. The left ventricle pumps the blood into the aorta through the whole body. Therefore, it is the strongest of the four heart chambers and it has the thickest wall, which makes it easier to image. All data was measured for research done to gain insight in the changes in the fibrous structure of the heart wall after an infarct [5]. This analysis may lead to a better understanding of the remodeling process that takes place after the infarct. Eventually it can help in developing better treatments for cardiac ischemia.

Current methods for evaluating the structure of the heart employ color coding of the helix angle in one slice of the data, as is shown in figure 5(a). Our method shows more global information than existing slice visualizations and conveys the fibrous structure in a more complete and more intuitive way. It is more complete, because with a single color-coded image it is not possible to visualize all components of the fiber directions. It is more intuitive because the visualization shows hair-like structures that people are used to seeing and interpreting.

In figure 6(a) we visualize an axial slice of a healthy heart. It clearly shows the big circular cavity the left ventricle, and its thick wall. The right ventricle can be seen on the bottom right. It has a much smaller cavity and a thinner wall. The color coding that was applied maps the x, y and z values of the local tangent of the fiber to RGB components. It can be seen that from both the inside and the out-

side of the wall of the left ventricle, when moving to the middle of the wall, the fiber orientation gradually changes from largely out-of-plane to in-plane. In the middle of the heart-wall, the fibers follow a circular pattern. The latter cannot be visualized using 2D slice coloring of the helix angle only, as was shown in figure 5(a). Using our method, separate illustrations for in-plane and out-of-plane components of the fiber orientation are no longer necessary. This is considered a big advantage by the users. They use the visualization to get an overview of the data in order to select regions of interest that require further analysis. Also, our methods work well to gain insight in local fiber orientations and are preferred over glyphing methods.

Figures 6 (b)-(d) show results for infarcted hearts at 7 and 28 days after infarction. Figure 6(b) shows a heart slice at 7 days after infarction. The infarcted area is on the left. When compared with figures 5 and 6(a), it can be seen that the middle of the heart wall in the infarcted area, which shows a clear circular pattern in healthy hearts, is thinner. Also, the overall shape of the heart-wall in the infarcted area has become more irregular. Two different slices of two hearts scanned at 28 days after infarction are shown in figures 6(c) and 6(d). Figure 6(d) shows a long-axis slice, as opposed to all other figures which show short-axis slices. It can be clearly seen in this figure that the heart wall in the infarcted area, at the bottom of the image, has become much thinner than the rest of the heart wall. Also, the structure of the fibers in the infarcted area is more irregular. This can also be seen in figure 6(c). In addition, figures 6(b) and 6(c) show the local *FA* using color coding. The red areas appear mainly in the infarcted regions. This indicates that infarcted tissue is more anisotropic than tissue in non-infarcted areas. This appears contradictory because the irregularity of the fibers seems to indicate *less* structure in those areas. However, it can be explained by the formation of collagen fibers which strengthen the damaged regions in order to avoid rupture. DTI measurements of these collagen fibers give higher anisotropy values, while they are less structured. This was confirmed using histology.

The proposed visualization depends a lot on the ability of the user to interact with the data and to change visualization parameters in real-time. In order to achieve this interactivity, the lighting and shadowing were implemented using shaders that run directly on the GPU. The rendering performances for several datasets are listed in table 1. The measurements were made on a 3.2 GHz Pentium 4 PC with 1 GB of RAM and a GeForce 7800 GTX 256MB graphics card. Using line lighting and shadowing, the listed datasets with under 1M line segments show framerates between 15 and 53 FPS. This is enough to ensure interactive viewing. For comparison, we also list the performance when rendering the same datasets using polygonal tubes with six sides, as shown in figure 4(b). As can be seen, the proposed methods outperform the tube approach. Videos showing the interaction, and additional images, can be downloaded from http://timpeeters.com/research/vmv2006/.

5 Conclusions and future work

Our work was inspired by techniques for the rendering of human hair. With the techniques presented, it is possible to visualize denser sets of fibers, while the structure of the fibers is more apparent. The lighting of the fibers improves the perception of shapes. The casting of shadows by the fibers onto each other shows which fibers are in front and which are behind in an intuitive way. This also shows the coherencies among fibers. We showed that the proposed slice visualization is useful for getting insight in DTI datasets of the heart. It shows the fibrous structure of slices of the heart in an intuitive way. Furthermore, it allows for visualization of extra properties such as *FA* using color coding, in combination with the fiber orientations. Our users showed that this allows for easy inspection of the fibrous structure of healthy hearts, and to detect changes in ischemic hearts.

There are more hair-rendering techniques that can be applied to the visualization of DTI fibers. Mallo et al. propose a more complex method for illuminating lines [10] that can give better results in some cases. There are improved shadow mapping techniques, such as deep shadow maps [9] and opacity shadow maps [8], that were developed especially for the rendering of hair-like structures. The application of these techniques needs to be evaluated in the future.

We will also link DTI fibers with models or in-vivo MRI measurements of strain in the heart wall in order to relate structural changes caused by ischemia to the functioning of the heart. This can help

#fibers	total #line segments	FPS no lighting	FPS line lighting	FPS light+shadow	FPS tubes	Figure(s)
2744	50707	800	139	53	24	6(c)
4143	74578	550	97	36	17	6(d)
8354	96288	375	74	29	14	6(b)
4055	103575	425	68	26	11	6(a)
15105	177198	206	40	16	6.7	5, 4
1493	1006774	25	6.6	2.4	1.1	3
1660	1511642	36	4.4	1.7	0.7	2

Table 1: Dataset size and performance in frames per seconds (FPS) for rendering with line lighting and shadow mapping. The datasets are ordered by the number of line segments. Measurements were made using a 1024×768 viewport and a 4096×3072 shadow map. Tube rendering results were included for comparison.

to improve the treatment of heart diseases such as heart failure caused by the remodeling of the heart after an ischemic infarction.

Acknowledgements

We thank the Biomedical NMR group, and especially Annemiek Bouts, of the Dept. of Biomedical Engineering of the Technische Universiteit Eindhoven for the datasets.

This study was financially supported by the Dutch BSIK program entitled Molecular Imaging of Ischemic heart disease (project number BSIK 03033).

References

[1] D. Akers, A. Sherbondy, R. Mackenzie, R. Dougherty, and B. Wandell. Exploration of the brain's white matter pathways with dynamic queries. In *Proceedings of IEEE Visualization 2004*, pages 377–384. IEEE Computer Society, 2004.

[2] R.H. Anderson, S.Y. Ho, K. Redmann, D. Sanchez-Quintana, and P.P. Lunkenheimer. The anatomical arrangement of the myocardial cells making up the ventricular mass. *European Journal of Cardio-Thoracic Surgery*, 28:517–525, 2005.

[3] D.C. Banks. Illumination in diverse codimensions. In *SIGGRAPH '94*, pages 327–334. ACM Press, 1994.

[4] J. Blaas, C.P. Botha, B. Peters, F.M. Vos, and F.H. Post. Fast and reproducible fiber bundle selection in DTI visualization. In *Proceedings of IEEE Visualization 2005*, pages 59–64, 2005.

[5] A.A. Bouts. MR diffusion tensor imaging of left ventricular remodeling following myocardial infarction in mice. Master's thesis, Eindhoven University of Technology, 2006.

[6] Y. Jiang, K. Pandya, O. Smithies, and E.W. Hsu. Three-dimensional diffusion tensor microscopy of fixed mouse hearts. *Magnetic Resonance in Medicine*, 52:453–460, 2004.

[7] J. T. Kajiya and T. L. Kay. Rendering fur with three dimensional textures. In *SIGGRAPH '89*, pages 271–280. ACM Press, 1989.

[8] T.-Y. Kim and U. Neumann. Opacity shadow maps. In *Proceedings of the 12th Eurographics Workshop on Rendering Techniques*, pages 177–182. Springer-Verlag, 2001.

[9] T. Lokovic and E. Veach. Deep shadow maps. In *SIGGRAPH '00*, pages 385–392. ACM Press/Addison-Wesley Publishing Co., 2000.

[10] O. Mallo, R. Peikert, C. Sigg, and F. Sadlo. Illuminated lines revisited. In *Proceedings of IEEE Visualization 2005*, pages 19–26, 2005.

[11] P. Schmid, T. Jaermann, P.F. Boesinger, P.P. Lunkenheimer, C.W. Cryer, and R.H. Anderson. Ventricular myocardial architecture as visualized in postmortem swine hearts using magnetic resonance diffusion tensor imaging. *European Journal of Cardio-thoracic Surgery*, 27:468–474, 2005.

[12] D. Stalling, M. Zockler, and H.-C. Hege. Fast display of illuminated field lines. *IEEE Transactions on Visualization and Computer Graphics*, 3(2):118–128, 1997.

[13] A. Vilanova, G. Berenschot, and C. van Pul. DTI visualization with streamsurfaces and evenly-spaced volume seeding. In *Joint EUROGRAPHICS - IEEE TCVG Symposium on Visualization*, 2004.

[14] A. Vilanova, S. Zhang, G. Kindlmann, and D. Laidlaw. An introduction to visualization of diffusion tensor imaging and its applications. In J. Weickert and H. Hagen, editors, *Visualization and Processing of Tensor Fields*, Mathematics and Visualization, chapter 7, pages 121–153. Springer, 2005.

[15] A. Wenger, D.F. Keefe, S. Zhang, and D.H. Laidlaw. Interactive volume rendering of thin thread structures within multivalued scientific data sets. *IEEE Transactions on Visualization and Computer Graphics*, 10(6):664–672, 2004.

[16] L. Williams. Casting curved shadows on curved surfaces. In *SIGGRAPH '78*, pages 270–274. ACM Press, 1978.

[17] A. Woo, P. Poulin, and A. Fournier. A survey of shadow algorithms. *IEEE Transactions on Computer Graphics and Applications*, 10(6):13–32, 1990.

[18] L. Zhukov and A. H. Barr. Heart-muscle fiber reconstruction from diffusion tensor MRI. In *Proceedings of IEEE Visualization 2003*, pages 597–602. IEEE Computer Society, 2003.

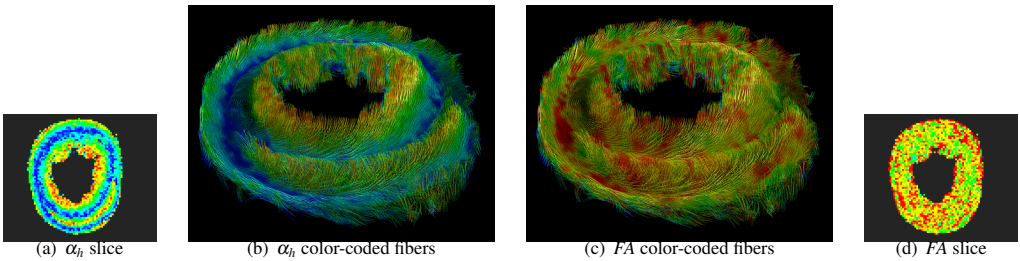

(a) α_h slice (b) α_h color-coded fibers (c) *FA* color-coded fibers (d) *FA* slice

Figure 5: (a), (b): Color coding of α_h. Blue indicates in-plane fibers, red is out-of-plane. (b), (c): Lighting and shadowing of lines combined with color coding of helix angle (α_h) and fractional anisotropy (*FA*). (c), (d): Color coding of *FA*. Green indicates small values for *FA* and red indicates large values.

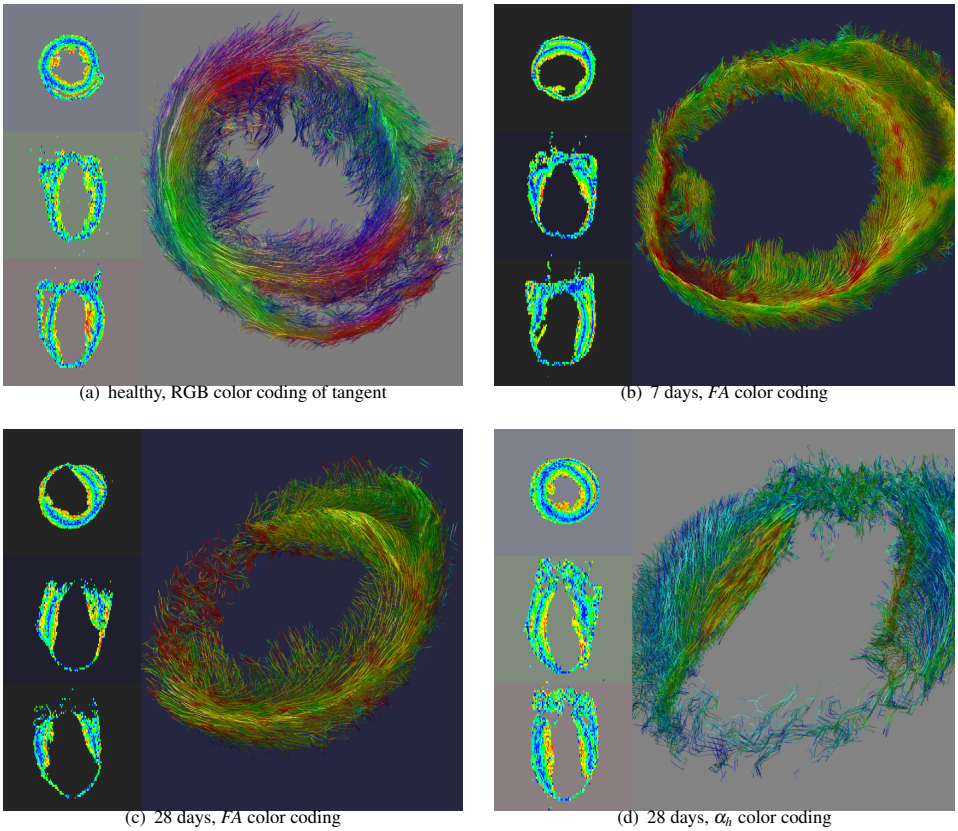

(a) healthy, RGB color coding of tangent (b) 7 days, *FA* color coding

(c) 28 days, *FA* color coding (d) 28 days, α_h color coding

Figure 6: Ischemic hearts 7 and 28 days after infarction. Selected saggital, coronal and axial slices are shown with α_h color coding on the left in each image. In (b) and (c), green indicates small values for *FA* and red indicates large values. Yellow indicates intermediate values.